

Stages of relaxation of patterns and the role of stochasticity in the final stage

Shaowen Hu¹, Daniel I Goldman^{2,7}, Donald J Kouri³, David K Hoffman⁴, Harry L Swinney⁵ and Gemunu H Gunaratne^{6,8}

¹ Department of Chemistry, University of Houston, Houston, TX 77204, USA

² Center for Nonlinear Dynamics, University of Texas at Austin, Austin, TX 78712, USA

³ Departments of Chemistry, Physics and Mathematics, University of Houston, Houston, TX 77204, USA

⁴ Department of Chemistry and Ames Laboratory, Iowa State University, Ames, Iowa 50011, USA

⁵ Center for Nonlinear Dynamics and Department of Physics, University of Texas at Austin, Austin, TX 78712, USA

⁶ Department of Physics, University of Houston, Houston, TX 77204, USA

E-mail: gemunu@uh.edu

Received 14 January 2004, in final form 21 April 2004

Published 21 May 2004

Online at stacks.iop.org/Non/17/1535

DOI: 10.1088/0951-7715/17/4/021

Recommended by J Lega

Abstract

The disorder function formalism (Gunaratne *et al* 1998 *Phys. Rev. E* **57** 5146) is used to show that pattern relaxation in an experiment on a vibrating layer of brass beads occurs in three distinct stages. During stage I, all length scales associated with moments of the disorder grow at a single universal rate, given by $L(t) \sim t^{0.5}$. In stage II, pattern evolution is non-universal and includes a range of growth indices. Relaxation in the final stage is characterized by a single, non-universal index. We use analysis of patterns from the Swift–Hohenberg equation to argue that mechanisms that underlie the observed pattern evolution are linear spatio-temporal dynamics (stage I), nonlinear saturation (stage II), and stochasticity (stage III).

PACS numbers: 05.70.Ln, 82.40.Ck, 47.54.+r

1. Introduction

Analysis of structures far from equilibrium and their evolution has led to the development of many novel concepts and techniques [1]. These structures are formed in driven, dissipative

⁷ Present address: Department of Integrative Biology, The University of California at Berkeley, Berkeley, CA 94720-3140.

⁸ Also at: The Institute of Fundamental Studies, Kandy 20000, Sri Lanka.

physical systems, and hence the underlying processes are irreversible. Further, their dynamics is typically nonlinear, and consequently, the systems exhibit sensitive dependence on initial states [2]; i.e. differences between nearly identical patterns increase in time. However, although dissipative structures formed from distinct initial states differ in detail, they are seen to share features that depend only on control parameters of the physical system. For example, domain sizes in multiple realizations of a pattern forming experiment, conducted under identical external conditions, have similar distributions.

Prigogine and others proposed the use of ensembles of solutions of a given physical system to conduct a statistical analysis of such dissipative structures and their variations with changes in external control parameters [3–6]. It is important to note that, unlike in the case of equilibrium statistical mechanics, the dynamics is not ergodic; thus, spatio-temporal dynamics of one member of the ensemble does not need to pass through the phase-space neighbourhood of another. A statistical description of dissipative structures formed in a given class of physical systems requires characteristics that are (nearly) identical for all members of the ensemble. The availability of multiple characteristics can be expected to provide a more comprehensive statistical description of the ensemble. However, the identification of such measures is a non-trivial task.

We consider properties of large aspect ratio patterns that are formed via spontaneous symmetry breaking from a noisy, but otherwise structureless initial state. Patterns are generated when an external control parameter crosses a threshold, initiating a local bifurcation to a periodic array; these arrays are, typically, striped, square, triangular or hexagonal [1]. However, due to translational and rotational invariances of the underlying system, the location and orientation of these local patches are not synchronized over the entire domain. As they grow, these patches compete with each other to produce complex patterns seen in experimental and model systems [7–13] (see figures 1, 6 and 9). These structures, whose details are sensitively dependent on the initial state, can be considered to belong to the ensemble of patterns.

Assume that such a spatio-temporal pattern can be represented by a scalar field $u(\mathbf{x}, t)$. Several functionals of $u(\mathbf{x}, t)$ have been proposed as measures to be used in statistical descriptions. Most of these are modelled on related quantities from equilibrium statistical mechanics. The width of the structure factor $S(t)$ [13–15] (i.e. the width of the peak in the azimuthal average of $\langle \hat{u}(\mathbf{k}, t)\hat{u}(-\mathbf{k}, t) \rangle$) is one of the more frequently studied examples. It has been shown that the evolution of a pattern from a noisy initial state consists of two distinct stages [14]: $S(t) \sim t^{-\frac{1}{2}}$ is obeyed until the peak amplitude of the field $u(\mathbf{x}, t)$ saturates, beyond which time the pattern coarsens and the decay becomes slower. For the (variational) Swift–Hohenberg equation, Elder *et al* [13] and Hou *et al* [16] found that, during this second stage, $S(t)$ decreased as $t^{-0.20}$ for noise-free dynamics and at a faster rate $t^{-0.25}$ when the dynamics was noisy. Cross and Meiron studied deterministic spatio-temporal dynamics in both variational and non-variational systems and found that $S(t) \sim t^{-0.2}$ [15]. Additional quantities have been introduced to describe the second relaxation region. Hou *et al* [16] measured cumulative domain wall length as a function of time. For noise-free (respectively noisy) dynamics, it was shown to decay as $t^{-0.25}$ (respectively $t^{-0.30}$). Cross and Meiron [15] introduced a stripe orientation correlation field and showed that it decayed as $t^{-0.24}$ for variational dynamics and at a much faster rate $t^{-0.51}$ for non-variational dynamics. For the latter case, these results provide strong evidence for the presence of a second length scale [15].

Note that in the second relaxation stage of a given model system, distinct measures (which probe multiple features of a pattern) decay at different rates. A systematic way to study such variations is to define a field to quantify the ‘local’ disorder, and to use multiple moments of this field to construct a family of characteristics to describe the dynamics of various length scales associated with the pattern [17]. Such a class appropriate for labyrinthine patterns,

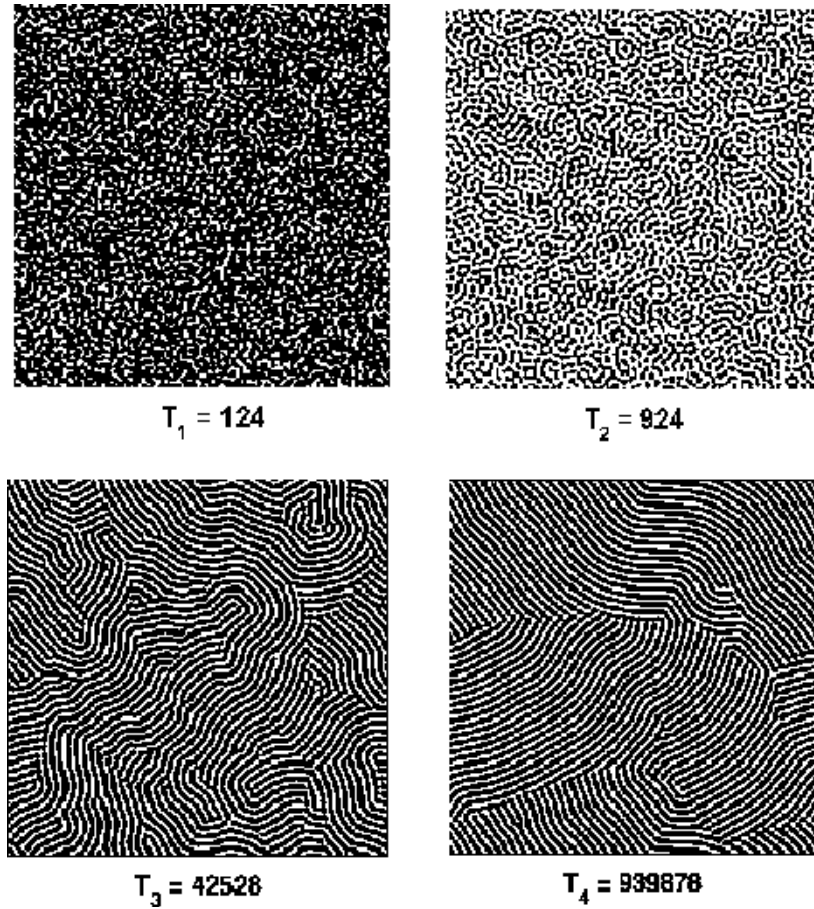


Figure 1. Four snapshots of the spatio-temporal dynamics of a random initial state ($|u(\mathbf{x}, t)| < 0.001$) under equation (2) with $D = 0.01$, $\epsilon = 0.1$, $k_0 = \frac{1}{3}$, $\nu = 0$, $\gamma = 2$, and $F = 0$. Times $T_1 = 124$ and $T_2 = 924$ are in stage I, and $T_3 = 42, 528$ and $T_4 = 939, 878$ are in stage II. Each side of the domain is $96\pi/k_0$, and periodic boundary conditions are imposed on the model. The peak of the radial projection of the power spectrum in the spatio-temporal dynamics relaxes to k_0 .

referred to as the disorder function, has been introduced [18, 19]. It is defined as

$$\delta(\beta, t) = \left[\frac{(2 - \beta) \int d^2x |(\Delta + k^2)u(\mathbf{x}, t)|^\beta}{\int d^2x \langle |u(\mathbf{x}, t)| \rangle^\beta} \right] / k^{2\beta}, \quad (1)$$

where k is the wavevector associated with the local planform, $\langle |u(\mathbf{x}, t)| \rangle$ denotes the mean of $|u(\mathbf{x}, t)|$, $\int d^2x$ is the area of the pattern, and $\delta(\beta, t)$ ($0 \leq \beta < 2$) has been normalized to be scale invariant. In this definition, the field used to quantify the local disorder is the magnitude $|(\Delta + k^2)u(\mathbf{x}, t)|$ of the Helmholtz operator. The integrand is non-zero at locations where the local wave-number deviates from its global mean k , and those where the planforms are curved. (The latter claim can be shown by considering a region of stripes with a radius of curvature r ; i.e. $u(\mathbf{x}, t) \sim \exp(ikr)$. There $|(\Delta + k^2)u(\mathbf{x}, t)| \sim k/r$.) Distinct ‘moments’ β can be used to emphasize particular features of a pattern; for example, large values of β provide a higher weight to defects [18, 20]. Methods to calculate $\delta(\beta, t)$ for (noisy) experimental patterns have been introduced [21]. In this paper, we will describe spatio-temporal dynamics

using $\delta'(\beta, t) = \delta(\beta, t)^{1/\beta}$. As can be easily seen, for each β , $\delta'(\beta, t)$ is the ratio of a wave number associated with the moment β of the Helmholtz operator and k .

The disorder function analysis of the evolution of patterns under model spatio-temporal dynamics from an initially noisy state reveals the presence of two stages [19], consistent with the analysis of $S(t)$ [13]. It is found that during the first stage spatio-temporal dynamics is essentially linear, and $\delta'(\beta, t) \sim t^{-\sigma_1}$, where $\sigma_1 = \frac{1}{2}$ is a universal exponent [19]. Thus, the wave number associated with each moment β reduces at a rate $t^{-\sigma_1}$, and the corresponding length scale grows as t^{σ_1} . The second stage, domain-coarsening, exhibits more complex behaviour. The relaxation is described by $\delta'(\beta, t) \sim t^{-\sigma_{\text{II}}(\beta, t)}$ [20]. Unlike σ_1 , $\sigma_{\text{II}}(\beta, t)$ is model dependent; in particular, the rate of relaxation depends on the coefficient of non-variational terms [19]. In addition, wave numbers associated with multiple moments decay with rates that depend on β .

These conclusions were recently validated in a set of experiments on pattern formation in a vibrating layer of brass beads [20]. However, the experiments showed, in addition, that for very long times the patterns reach a third stage; here, the indices $\sigma_{\text{III}}(\beta, t)$ are independent of β , but their common value depends on control parameters of the experiment. The work reported in this paper shows that the presence of this final stage in systems far from the onset of patterns is one observable consequence of stochasticity in the underlying spatio-temporal dynamics. The results complement recent demonstrations on effects of noise in systems close to the onset of patterns [22, 23].

2. Model system and analysis

The model system used in our studies is an extension of the Swift–Hohenberg equation [1], which describes the dynamics of a scalar field $u(\mathbf{x}, t)$ via

$$\frac{\partial u}{\partial t} = D \left(\epsilon - (1 + k_0^{-2} \Delta)^2 \right) u - \gamma u^3 - \nu (\nabla u)^2 + \eta(\mathbf{x}, t). \quad (2)$$

D sets the rate of diffusion, ϵ is the distance from pattern onset, ν is the strength of a non-variational term [19], and k_0 is the wave number of the underlying planform. η is a stochastic term such that $\langle \eta(\mathbf{x}, t) \eta(\mathbf{x}', t') \rangle = F \delta(\mathbf{x} - \mathbf{x}') \delta(t - t')$, F being the strength of the noise; $\eta \neq 0$ and $\eta = 0$ represent stochastic and deterministic spatio-temporal dynamics. For suitable control parameters, random initial states (whose amplitude is chosen to be much smaller than the saturated peak amplitude of the field) evolve to patterns under equation (2). Several snapshots from such an evolution under deterministic dynamics are shown in figure 1.⁹

The behaviour of $\delta(1.0, t)$ corresponding to this spatio-temporal dynamics is shown in figure 2. Statistical variation between values of $\delta(1.0, t)$ in nominally identical patterns—i.e. those with the same control parameters, but different initial states—is negligible [19]. $\delta(1.0, t)$ exhibits an initial rapid decay followed by a much slower relaxation. During stage I, $\langle |u(\mathbf{x}, t)| \rangle$ is significantly smaller than its value at large times; hence, spatio-temporal dynamics can be approximated by the linear partial differential equation

$$\frac{\partial u}{\partial t} = \left(\epsilon - (1 + k_0^{-2} \Delta)^2 \right) u. \quad (3)$$

The Fourier transform of $u(\mathbf{x}, t)$ satisfies

$$\hat{u}(\mathbf{k}, t) = \hat{u}(\mathbf{k}, 0) \exp \left(\epsilon t - \left(1 - \frac{\mathbf{k}^2}{k_0^2} \right)^2 t \right). \quad (4)$$

⁹ Methods used to integrate these spatio-temporal dynamics are described in [19].

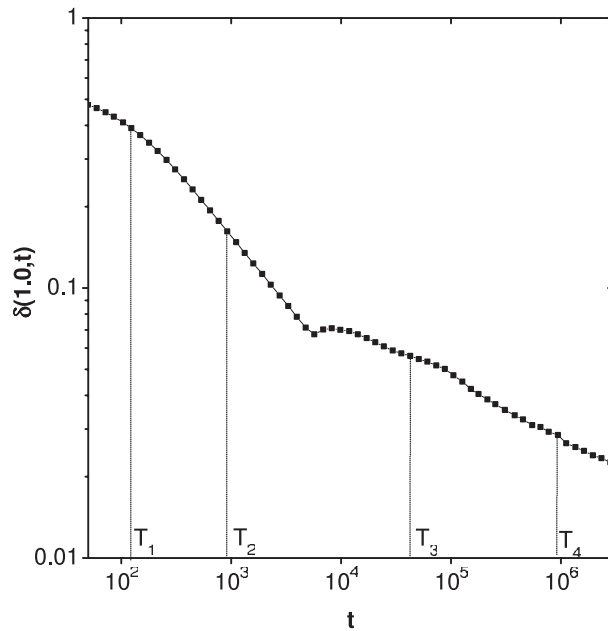


Figure 2. The behaviour of $\delta(1.0, t)$ for the spatio-temporal dynamics shown in figure 1. The presence of two distinct stages of relaxation can clearly be observed.

For a given noisy initial state, this solution can be used to evaluate integrals in equation (1). It is found that $\langle |u(x, t)| \rangle \sim e^{\epsilon t} t^{-1/4}$ and (for values of t that are not very small) $\int d^2x |(\Delta + k_0^2)u(x, t)|^\beta \sim e^{\beta \epsilon t} t^{-3\beta/4}$ ¹⁰. Consequently, $\delta(\beta, t) \sim t^{-\beta/2}$ and $\sigma(\beta, t) = \sigma_I = \frac{1}{2}$.

Results shown in figure 2 can be used to compute $\sigma(\beta, t)$. At a given time t , we use the five nearest points (t and the closest two points on both sides) to calculate the slope of the curves $\log \delta(\beta, t)$ versus $\log t$ using a least squares fit. As shown in figure 3, this analysis confirms that $\sigma_I(\beta, t) = \frac{1}{2}$ during stage I.

The onset of stage II coincides with the saturation of the peak value of the field $u(\mathbf{x}, t)$ and beyond this time the relaxation of $\delta(1.0, t)$ is slower. Further, as seen from figure 3, $\sigma(\beta, t)$ varies both with t and β . The variation with β implies that the wave numbers associated with $\delta'(\beta, t)$ decay at rates that depend on β ; i.e. length scales associated with multiple features of these patterns grow at different rates [20]. The spatio-temporal dynamics shown in figure 1 retains this feature even for very large times, when the pattern consists of a few large domains.

Typically, $\sigma(\beta, t)$ is a monotonically decreasing function of β during stage II; thus, the mean distance between defects ($\beta \rightarrow 2$ [18]) grows at a slower rate than (for example) the mean curvature or domain size. Exceptions occur during the removal of defect(s) or small domains from a pattern. These events can be identified by a sudden rapid decrease in $\delta(\beta, t)$, an example of which is seen near T_4 in figure 2. Figure 4 shows the pattern prior to and following the absorption of a small domain into a larger one. The behaviours of $\delta(1.0, t)$ and $\sigma(\beta, t)$ during this metamorphosis are shown in figures 5(a) and (b). It can be seen that $\sigma(\beta, t)$ which is monotonic before and after the change takes on a more complex form during the transition. This method can be used to identify domain disappearance even when it is difficult to recognize the change visually (as often happens in patterns with a large number of domains).

¹⁰ These integrals cannot be calculated due to the nonanalyticity of $|x|$. The values for the analytic case, $\beta = 2$, are easily obtained using Parseval's theorem.

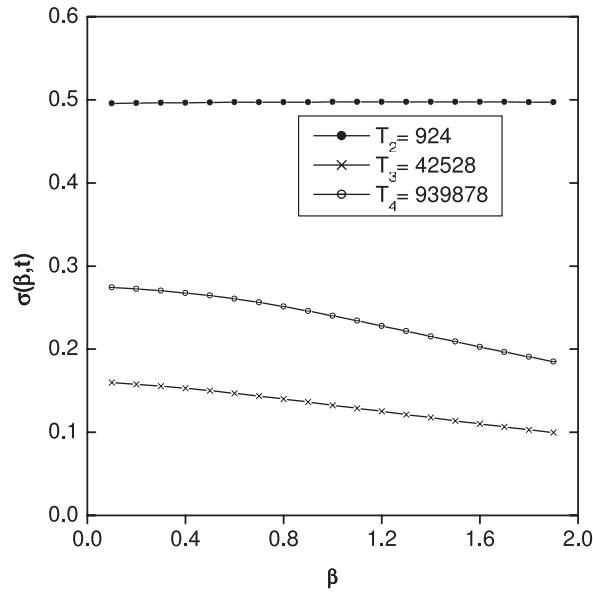


Figure 3. The behaviour of the function $\sigma(\beta, t)$. During the domain forming stage $\sigma(\beta, t) = \frac{1}{2}$, while it is β dependent in the domain coarsening stage. As in the example shown, $\sigma(\beta, t)$ also varies with time during the second stage.

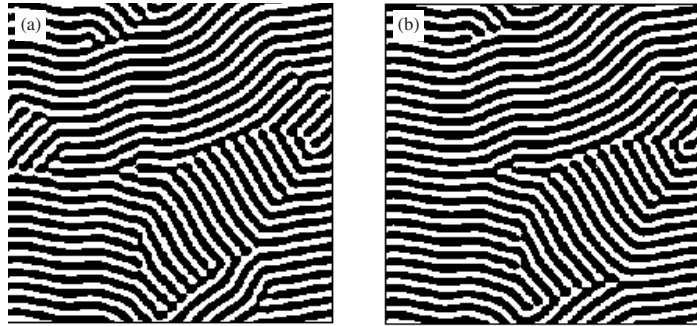


Figure 4. Sharp reductions in $\delta(\beta, t)$ (similar to that near T_4 in figure 1) correspond to the disappearance of domains or defects. The images (a) before and (b) after such an event. It is found that $\sigma(\beta, t)$ fails to monotonically decrease during and immediately following such events.

3. Results from the experiment

The pattern forming experiments were conducted with 0.165 mm bronze spheres contained in a vertically oscillated circular container with a diameter of 140 mm [11, 20]. The layer is four particle diameters deep, and the cell is evacuated to 4 Pa so that hydrodynamic interaction between the grains and surrounding gas is negligible. The control parameters are the frequency f of the sinusoidal oscillations and the peak acceleration of the container relative to gravity, $\Gamma = (2\pi f)^2 A^2 / g$, where A is the amplitude of the oscillation and g is the gravitational acceleration. As f and Γ are changed, a variety of temporally subharmonic patterns including locally square, striped, or hexagonal patterns are observed [11]. The textures analysed consisted of patterns with square planforms [20].

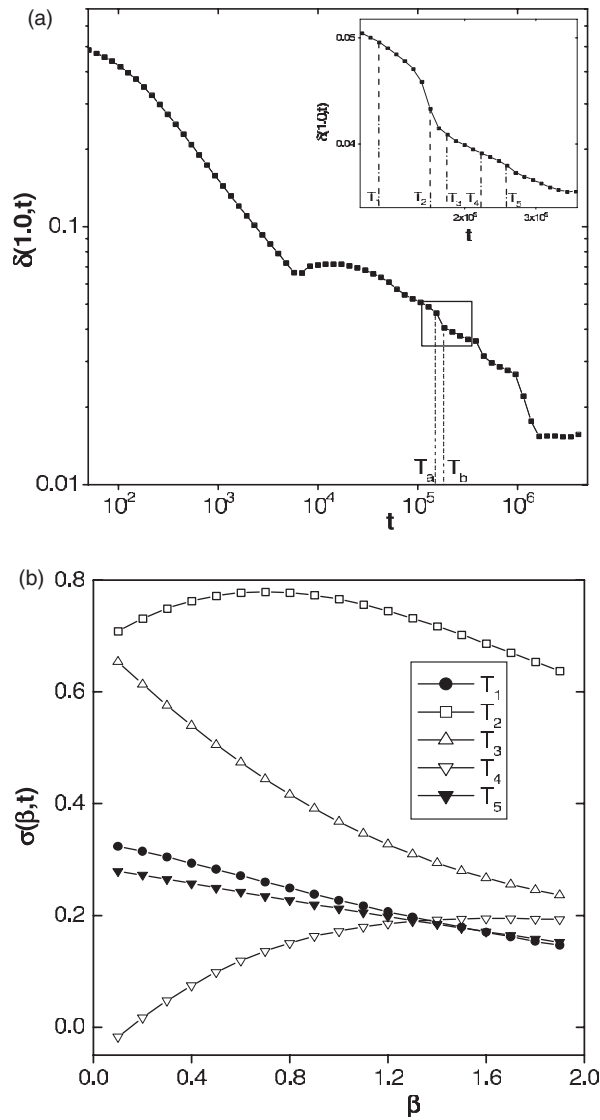


Figure 5. The behaviour of $\delta(\beta, t)$ and $\sigma(\beta, t)$ during the removal of a small domain. Note that, while $\sigma(\beta, t)$ decreases monotonically before the event and following the relaxations of the neighbourhood, it exhibits more complex behaviour during the event.

The granular surface is visualized by illuminating the cell using a ring of LEDs surrounding the cell and is strobed at the drive frequency of the container. The light is incident at low angles and the scattering intensity is a nonlinear function of the height of the layer; scattering from peaks (valleys) creates bright (dark) regions. This intensity field is used to represent the structures [20].

Figure 6 shows four snapshots during the evolution of an experimental pattern, and figure 7 shows the corresponding behaviour of $\delta(1.0, t)$. Stages I and II, analogous to those seen in patterns of the model system, can be observed. It was confirmed that the onset of stage II corresponded to the saturation of the peak amplitude [20]. Using the leftmost interval shown

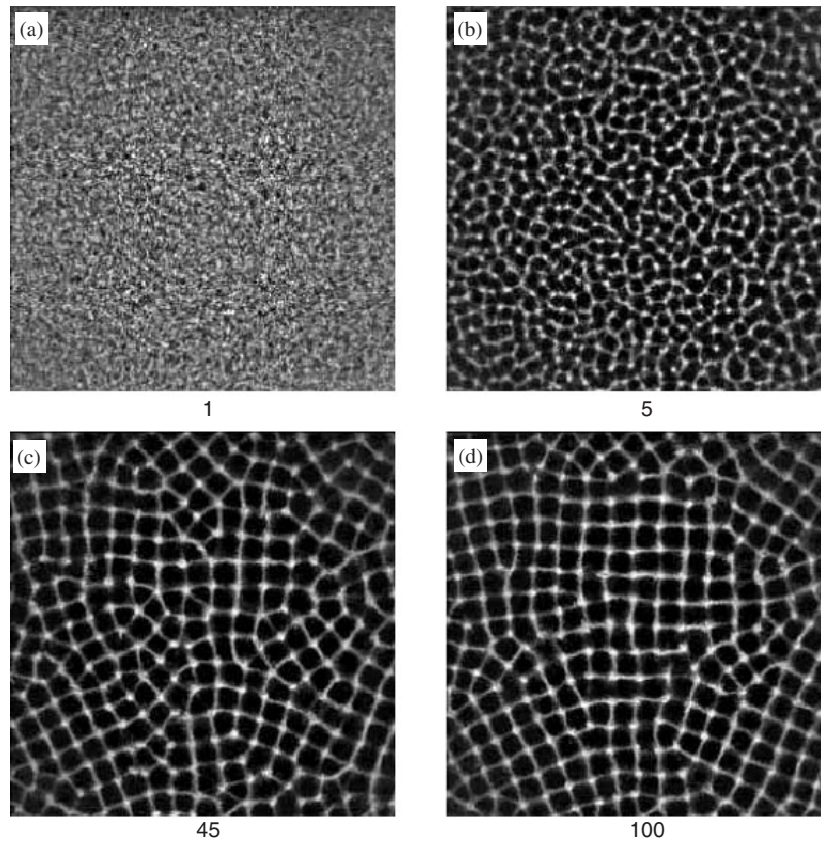


Figure 6. The time evolution of an oscillated layer of grains following a rapid change in peak acceleration of the container from $2.2g$ to $3.0g$. Below the onset of patterns (which occurs at approximately $2.5g$), the layer is featureless but noisy while above onset defect-free square patterns are stable. The numeral below each snapshot indicates the number of layer–plate collisions after the last layer take-off before the acceleration was changed. The oscillation frequency in this experiment is $f = 27$ Hz.

in figure 7, the evolution during stage I was shown to be consistent with $\sigma(\beta, t) = \frac{1}{2}$, although there were insufficient data points for the result to be conclusive [20]. Beyond this stage, the relaxation was much slower, and $\sigma(\beta, t)$ depends on β [20] (see figure 8). However, it was observed that at much longer times (e.g. during the rightmost interval in figure 7) the patterns reach a stage where $\sigma(\beta, t)$ is independent of β , and its value is not the universal $\frac{1}{2}$ of the first stage (see figure 8).

4. Spatio-temporal dynamics under stochastic equations

Behaviour analogous to stage III in experimental patterns is not observed in the spatio-temporal dynamics such as that shown in figure 1, even at very large times when the pattern consists of a few domains. Clearly, one or more ingredients that are necessary for the description are missing from the model we have used. Candidates include non-variational terms, finite size effects and stochastic terms. Inclusion of non-variational terms have been shown to change the relaxation rates [15] and stochasticity is known to play a role in the dynamics near the onset

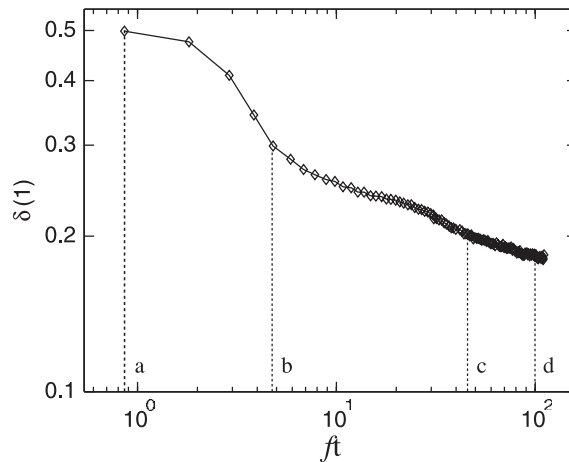


Figure 7. The time evolution of $\delta(1.0, t)$ for the sequence shown in figure 6. The abscissa is in units of the number of container oscillations from the last layer take-off before Γ was changed. The dashed lines indicate the time that snapshots in figure 6 were taken. Two distinct stages of pattern evolution are clearly visible; the initial rapid decay is consistent with $t^{-0.5}$, while the slower decay scales on average like $t^{-0.12}$. However, it is difficult to differentiate stages II and III from the dynamics of a single moment of the disorder function.

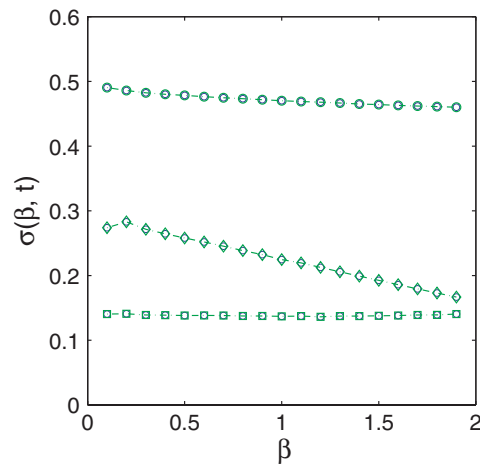


Figure 8. $\sigma(\beta, t)$ calculated for patterns shown in figure 7. Results from stages I, II, and III are shown as circles, diamonds and squares respectively. $\sigma(\beta, t)$ for the three stages were calculated using intervals shown in figure 6 (3–5 oscillations, 40–50 oscillations, and 85–105 oscillations following the initiation of the experiment). Now stages II and III can clearly be delineated.

(This figure is in colour only in the electronic version)

of patterns [23]. Further, only finite subdomains of the experimental system are analysed in contrast to the model system where periodic boundary conditions have been imposed.

Integration of the model system shows that neither the addition of non-variational terms ($\nu \neq 0$) to the spatio-temporal dynamics nor conducting the analysis on smaller sub-domains give a transition away from stage II, even at very large times. On the other hand, we find that the addition of stochastic terms does lead to such a transition, and that the new stage has characteristics described in the last section.

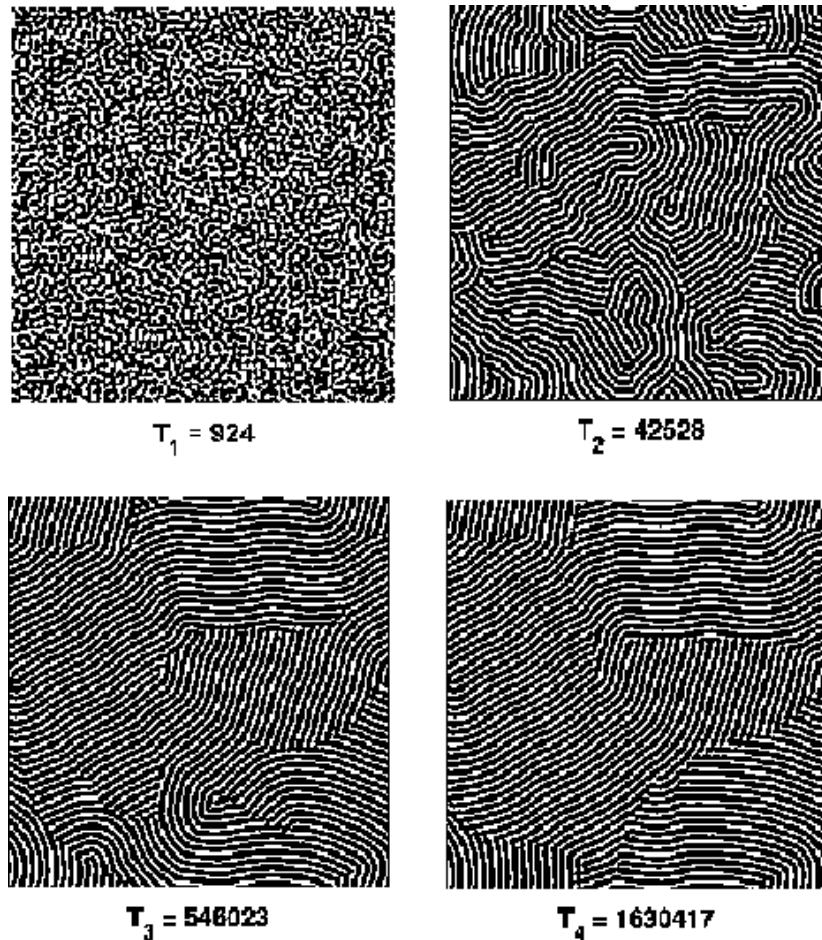


Figure 9. Four snapshots of the stochastic spatio-temporal dynamics of a random initial state ($|u(x, t)| < 0.001$) under equation (2) with $D = 0.01$, $\epsilon = 0.1$, $k_0 = \frac{1}{3}$, $\nu = 0.0$, $\gamma = 2.0$, and $F = 0.0005$. The $T_1 = 924$ is in stage I, $T_2 = 45, 528$ in stage II, and the last two $T_3 = 546, 023$ and $T_4 = 1, 630, 417$ are in stage III. Note that the pattern continues to evolve, albeit slowly, in stage III. As in figure 1, each side of the domain is $96\pi/k_0$, and periodic boundary conditions are imposed on the model. The peak of the radial projection of the power spectrum once again relaxes to k_0 .

Figure 9 shows four snapshots during the development of such a structure under the Swift–Hohenberg equation with stochastic terms (i.e. $F \neq 0$). The behaviour of $\delta(1.0, t)$ is qualitatively similar to figure 2. The principal difference that can be gleaned from the analysis of a single moment $\delta(\beta, t)$ is an increase in the decay rate, particularly in stage II. $\sigma(\beta, t)$ exhibits features that are similar to the corresponding noise-free dynamics; it is independent of β in stage I, but is a function of β following saturation of the field $u(x, t)$. However, at very large times, $\sigma(\beta, t)$ is once again seen to be independent of β , taking a value that depends on control parameters (see figure 10). It is also found that the onset of stage III advances with increasing intensity of the stochastic terms. For sufficiently large values of F the dynamics can move directly from stage I to III.

The implication of the β independence of σ_{III} is that all length scales associated with the pattern grow at the same rate during stage III. This assertion can be tested by studying the

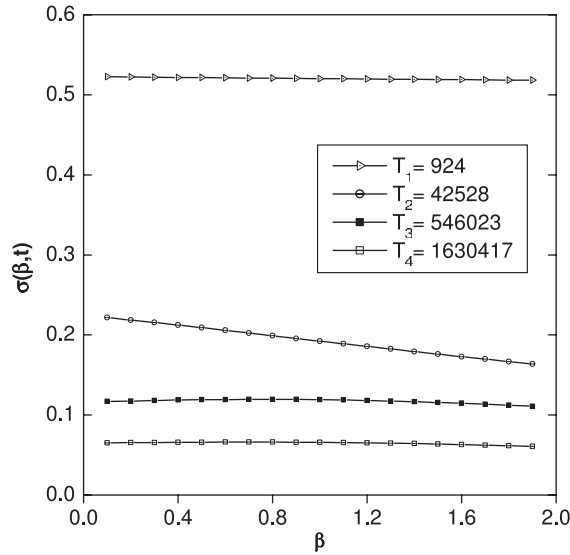


Figure 10. The behaviour of $\sigma(\beta, t)$ for stochastic spatio-temporal dynamics. Observe the presence of three distinct stages, as in experimental patterns.

relaxation of the width of the structure factor and the defect density. For the analysis, we used averages for four nominally identical runs with parameters given in figure 9. The mean decay rate of the width of the structure factor at time T_3 of figure 10 is found to be 0.12 ± 0.01 , in agreement with $\sigma_{\text{III}}(T_3)$. Second, the mean number of defects at T_3 is found to decrease like T^χ , where $\chi = -0.20 \pm 0.02$. The associated length scale (i.e. the mean distance between defects) grows with an index $\frac{1}{2}\chi$, once again consistent with the value of $\sigma_{\text{III}}(T_3)$.

5. Discussion and conclusions

We set out to compare and contrast pattern dynamics in distinct systems. It is important to note that such a task can only be achieved using ‘configuration independent’ characteristics, i.e. measures that depend on control parameters of the underlying system, and not on the (random) initial states. For complex patterns with local planforms such as stripes, squares or hexagons (e.g. figures 1, 6 and 9), such measures include the width of the structure factor [13, 15], defect density [16], length of domain boundaries [26], and the disorder function [18, 27].

Analysis of patterns generated in the Swift–Hohenberg equation and on a vibrating layer of brass beads shows that during early times all components of the disorder function relax as $t^{-0.5}$. We showed that the index can be obtained by noting that during this stage the intensity of the field representing the pattern is sufficiently small and hence the spatio-temporal dynamics can be considered to be linear. The saturation of the field is followed, in each case, by a second stage where the relaxation is non-universal and the growth indices $\sigma(\beta, t)$ are β dependent; the latter implies that the growth of distinct features of patterns occur at different rates. Experimental patterns exhibit a third stage at times very long compared to the vibrational period of the container [20], where $\sigma(\beta, t)$ is once again independent of β . It is not possible to differentiate it from stage II by analysing the behaviour of a single index; rather, it requires the use of the entire family of indices $\sigma(\beta, t)$. Unlike in stage I, the value of $\sigma(\beta, t)$ is not universal. Stage III is not present in spatio-temporal dynamics under the deterministic Swift–Hohenberg equation,

even when non-variational terms and finite-size effects are included. Our work suggests that the ingredient required to initiate stage III is stochasticity of the underlying spatio-temporal dynamics.

It should be noted that $\delta(\beta, t)$ was constructed to quantify disorder in patterns that consist of local planforms that satisfy the Helmholtz equation [27]. Structures formed in other systems, such as in the X–Y model [28], in spinodal decomposition [29], or in epitaxial growth [30] do not have such local planforms. Measures to conduct irreversible statistical analyses of such structures remain to be identified.

Acknowledgments

The authors would like to acknowledge discussions with M Shattuck. This research is supported by grants from the National Science Foundation (DJK, GHG), the R A Welch Foundation (DJK), the Office of Naval Research (GHG), and the Engineering Research Programme of the Basic Energy Sciences of the DOE (DIG, HLS). The numerical integrations reported were conducted using computers at the High Performance Computing Center at the University of Houston.

References

- [1] Cross M C and Hohenberg P C 1993 *Rev. Mod. Phys.* **65** 851
- [2] Egolf D and Greenside H 1995 *Phys. Rev. Lett.* **74** 1751
- [3] Petrosky T, Prigogine I and Tasaki S 1991 *Physica A* **173** 175
- [4] Petrosky T and Prigogine I 1993 *Proc. Natl Acad. Sci.* **90** 9393
- [5] Hasegawa H H and Saphir W C 1992 *Phys. Lett. A* **161** 471
- [6] Antoniou I and Tasaki S 1993 *J. Phys. A* **26** 73
- [7] Ouyang Q and Swinney H L 1991 *Nature* **352** 610
- [8] Heutmaker M S and Gollub J P 1987 *Phys. Rev. A* **35** 242
- [9] Bodenschatz E, de Bruyn J R, Ahlers G and Cannel D S 1991 *Phys. Rev. Lett.* **67** 3078
- [10] Rosenweig R E 1985 *Ferrohydrodynamics* (Cambridge: Cambridge University Press)
- [11] Melo F, Umbanhower P and Swinney H L 1993 *Phys. Rev. Lett.* **72** 172
- [12] Bestehorn M 1993 *Phys. Rev. E* **48** 3622
- [13] Elder K R, Viñals J and Grant M 1990 *Phys. Rev. A* **46** 7618
- [14] Schober H R, Allroth E, Schroeder K and Müller-Krumbhaar H 1986 *Phys. Rev. A* **33** 567
- [15] Cross M C and Meiron D I 1995 *Phys. Rev. Lett.* **75** 2152
- [16] Hou Q, Sasa S and Goldenfeld N 1997 *Physica A* **239** 219
- [17] Ruelle D 1978 *Statistical Mechanics, Thermodynamic Formalism* (Reading, MA: Addison-Wesley)
- [18] Feigenbaum M J 1987 *J. Stat. Phys.* **46** 919
- [19] Gunaratne G H, Jones R E, Ouyang Q and Swinney H L 1995 *Phys. Rev. Lett.* **75** 3281
- [20] Gunaratne G H, Ratnaweera A and Tennekone K 1999 *Phys. Rev. E* **59** 5058
- [21] Goldman D I, Shattuck M D, Swinney H L and Gunaratne G H 2002 *Physica A* **306** 180
- [22] Hoffman D K, Gunaratne G H, Zhang D S and Kouri D J 2000 *Chaos* **10** 240
- [23] Oh J and Ahlers G 2003 *Phys. Rev. Lett.* **91** 094501
- [24] Goldman D I, Swift J B and Swinney H L 2004 *Phys. Rev. Lett.* **92** 174302
- [25] Newell A C and Whitehead J A 1969 *J. Fluid Mech.* **38** 279
- [26] Segel L A 1969 *J. Fluid Mech.* **38** 203
- [27] Gunaratne G H 1993 *Phys. Rev. Lett.* **71** 1367
- [28] Gunaratne G H, Ouyang Q and Swinney H L 1994 *Phys. Rev. E* **50** 2802
- [29] Ouyang Q and Swinney H L 1991 *Chaos* **1** 411
- [30] Gunaratne G H, Hoffman D K and Kouri D J 1998 *Phys. Rev. E* **57** 5146
- [31] Bray A J 1994 *Adv. Phys.* **3** 357
- [32] Cahn J W and Hilliard J E 1958 *J. Chem. Phys.* **28** 258
- [33] Vvedensky D D, Zangwill A, Luse C N and Wilby M R 1993 *Phys. Rev. E* **48** 852